Diffeomorphic Surface-Based Registration for MR-US Fusion in Prostate Brachytherapy

Augustin Cosse[1]
[1] ICTEAM Institute, Université catholique de Louvain, Louvain-La-Neuve, Belgium
augustin.cosse@uclouvain.be

***Abstract*—In nowadays prostate interstitial brachytherapy, transrectal ultrasound guidance is typically used to localize the prostate and the rectum. However, the ability of ultrasound to distinct normal from cancer tissues is weak. In most treatments, the organ as a whole is thus irradiated, leading to numerous side effects such as urinary or sexual dysfunction. The quality of magnetic resonance images (MRI), on the other hand, has improved over the last few years and allows for an accurate delineation of the tumor [1]. This paper proposes a novel framework for MRI-US surface registration of the prostate and the rectum. The preoperative MRI is first segmented using a multiresolution graph-cut method. The intraoperative US image is manually segmented by the surgeon. The registration is then performed in two steps. In a first step, a bi-affine registration is performed on the surfaces of the rectum and the prostate using an expectation maximization iterative closest point method (EM-ICP). In the second step, non-rigid registration is applied to the distance maps resulting from the pre-registered surfaces. Our approach has been applied on 5 MR/US pairs and shows a relative independence between prostate and rectum motions.**

I. Introduction

Prostate cancer is the most frequent diagnosed malignancy in male over 50 years. In Europe in 2008, an estimated 382,000 cases were diagnosed while 90,000 deaths have occured in 2008 [2]. In prostate brachytherapy as well as in thermoablation therapy, ultrasound images are used to localize the organs [3]. However, the usefullness of this intraoperative visualization is compromised by the poor resolution of the images and the impossibility to localize the tumor. Indeed, transrectal ultrasound allows a correct identification of the position and boundaries of the prostate, but does not allow discriminating between normal and cancer tissue.

This paper proposes to register preoperative T2-weighted magnetic resonance images (MRI) and intraoperative transrectal ultrasound images (TRUS). T2-weighted images are images which show the spin-spin or transverse relaxation time of tissues. For more information concerning this first modality see for example [4], [5]. Information concerning ultrasound imaging can be found in [6].

MR/US registration is known to be challenging due to the very different nature of these two modalities. A few examples of such fusion have been proposed. Mitra et al [7] as well as Makni et al [8], propose to deal with this issue by means of thin plate splines. Martin et al [9] first segment prostate and rectum in both modalities and then use surface meshes in order to perform registration. Porter et al [10] use segmented MR and US vessels as landmarks together with a correlation scheme to define correspondences between the two images. Finally, Reynier et al [11] perform a registration of point sets.

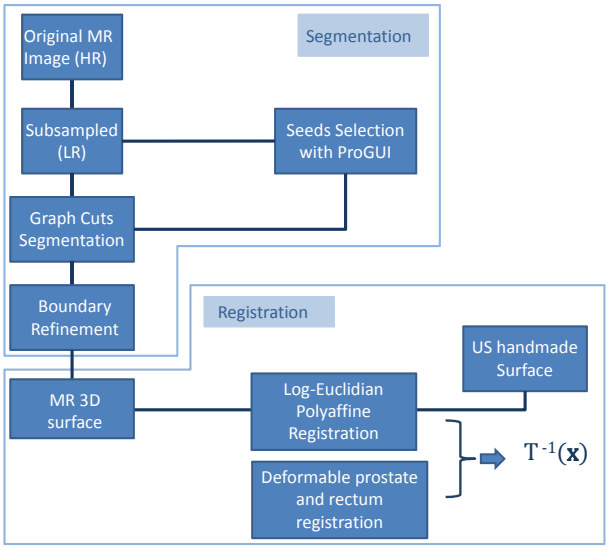

Fig. 1. In order to fuse the information of the MR and US images, we use a two-step process. In a first step, the organs are segmented in the preoperative MR image. In the second step the extracted surfaces are registered with manually defined segmentations in the US image.

This paper proposes a surface-based registration framework for MR/US fusion (see figure 1). Prostate and rectum surfaces are segmented from the MRI using an interactive multi-scale graph-cut method that extends the classical graph-cut segmentation [12], [13], [14], [15]. Corresponding surfaces in the US image are manually segmented by the surgeon. A log-euclidean polyaffine registration is then used to register the two surfaces. Each affine component is first estimated using an expectation maximization iterative closest point method (EM-ICP) [16]. The obtained affine transformations are then combined using the log-euclidian polyaffine framework (see [17]) in order to obtain a deformation field on the whole image. The deformed surfaces are encoded in as a distance map and a non-rigid registration is performed using as fixed image the US distance map and as moving image the distance map of the deformed MR image.

The rest of this paper is organized as follows. Section II introduces the different elements of the method, including the graph-cut segmentation, the EM-ICP log-euclidian polyaffine registration and the non-rigid registration. Section III presents

the segmentation and registration results on a set of MR/US validation pairs. Finally, Section IV concludes and presents some directions for future work.

II. Methods

The proposed method consists in 2 parts : (1) a MR segmentation step and (2) a MR-US surface registration step (cfr figure 1). Section II-A briefly explains how the segmentation is performed. Then, sections II-B and II-C review the registration scheme.

A. Graph-Cut Segmentation of the MRI

Graph-cut segmentation is an efficient method when the boundary cannot clearly be distinguished but when different textures and structures are present within an object [12]. Given an image with intensity $I(p)$ at voxel p and given three sets of predefined seeds O_B, O_P, O_R that belong to the background, the prostate and the rectum respectively, the graph-cut segmentation finds an optimal labeling function f that assigns label $f(p)$ to voxel p, minimizing some energy function. The optimization respects the hard constraint that $f(s) = l_j$ if $s \in O_j$ for $j = B, P, R$.

In this paper, we propose to minimize the following energy [12]:

$$E(f) = \sum_{\{p,q\} \in N} V_{p,q}(f(p), f(q)) + \lambda \sum_{p} R_p(f(p)), \qquad (1)$$

where N is the set of all pairs of adjacent voxels. The first term of (1) tends to assign the same label to adjacent voxels that have similar intensities:

$$V_{p,q}(f(p), f(q)) = \begin{cases} \exp\left(-\frac{(I(p)-I(q))^2}{2\sigma^2}\right) & \text{if } f(p) \neq f(q) \\ 0 & \text{otherwise.} \end{cases}$$

The second term of (1) tends to assign label l_j to p if $I(p)$ is close to the intensities of the seeds in O_j. Mathematically speaking, this term is the negative log-likelihood of the voxel intensity given that it would belong to $O_{f(p)}$:

$$R_p(f(p)) = -\log P(I(p)|O_{f(p)})$$

where the conditional probabilities are estimated by the intensity histogram of the corresponding set of seeds.

Graph-cut finds the global minimum of (1) based on the construction of a graph whose nodes correspond to the voxels of the image added to two super-nodes : the sink (t) and the source (s) (see figure 2) [18].
Let $\{l_1 = l_P, l_2 = l_R, l_3 = l_B\}$ be our labels. We label l_1 the voxels that belong to the prostate, those who belong to the rectum will be labeled l_2 and finally the background will get label l_3. Then, we build graph $\mathcal{G}$ as follows. As in [18], the set $\mathcal{V} = \{p_1, p_2, q_1, q_2, \ldots, s, t\}$ of vertices still contains a source s and a sink or terminal node t. Between those two terminal nodes, we define 3 edges t_1, t_2, and t_3 (*see* figure 2) for each voxel. Each edge thus corresponds to one particular label. Out of concern for clarity, we only represented part of the graph since normally p_1 has links with q_1, r_1, …, p_2 has links with q_2, r_2, …, *etc*. Edges weights are defined by $t_i^p = 1 + 2\sum_{q \in \mathcal{N}_p} W_{p,q} + R_p(x_p = i)$ for edges between p_i and p_{i+1} or between t (resp. s) and p_i and by the usual pairwise cost $W_{p,q} = \exp\left(-\frac{(I(p)-I(q))^2}{2\sigma^2}\right)$ for edges between p_i and q_i.

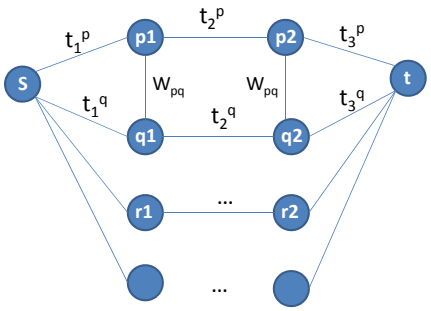

Fig. 2. In order to segment the image, a graph with nodes corresponding to voxels and edges encoding the similarity between voxels is built. The graph cut algorithm of [18] is then applied on this graph.

Doing this, the labeling associated with a cut is defined as follows : if the cut severs edge t_i^p we associate the label i to the voxel p. and the weight of t_i^p, $1+2\sum_{q \in \mathcal{N}_p} W_{p,q} + R_p(x_p = i)$ is added to the total cost. Moreover, if the cut severs edges t_i^p and t_j^q for $j < i$ then the weights of all edges $\mathcal{E}(p_k, q_k)$ for $j \leq k < i$ will be added to the total cost of the cut.

Although very effective, graph-cut is computationally expensive for tridimensional images. A two-step approach is therefore used. In a first step, graph-cut segmentation is performed on a low resolution version of the image. Once this first step has been completed, each low resolution voxel for which the assigned label differs from one of its neighbors is considered to be a boundary voxel. The corresponding nodes in the graph are split into sub-nodes corresponding to the voxels at higher resolution, and graph-cut is performed again on this multi-resolution graph (Fig. 3).

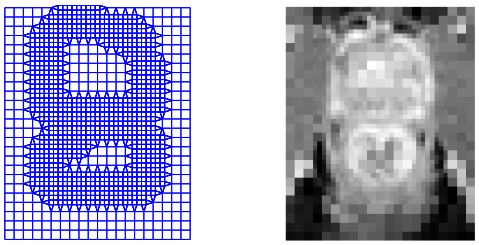

Fig. 3. (Left) Multi-resolution representation resulting from a first segmentation and the detection of the boundary. The high resolution content of the image is used only around the boundaries, making the second step of the graph-cut segmentation more efficient. (Right) The equivalent multi-resolution image in which voxels of the boundary have been resampled to the higher resolution.

B. Polyaffine Registration

Once the surfaces have been detected in the MRI by graph-cut, they can be registered onto the surfaces defined in the US image by the surgeon. In a first step, a polyaffine registration is performed, which affinely aligns the two pairs of surfaces independently and then combines the two transforms in the log-euclidean domain [17].

The two independent affine components (one for each organ) are estimated by EM-ICP [16]. This method has the advantage of being very robust to noise and of allowing the registration of partial surface onto a full surface. These properties are interesting in our case since noise is introduced by segmentation error in the graph-cut step.

Given two sets of points $\{s_i \; i = 1, \ldots, N_I\}$ and $\{m_j \; j = 1, \ldots, N_J\}$ corresponding to the organ in the MR and in the US images respectively, EM-ICP finds the transformation T that maximizes the log-likelihood of the correspondence between pairs of points. EM-ICP alternates between updating those probabilities considering T fixed (E-step) and optimizing the parameters of T given the correspondence probabilities (M-step). In other words, the E-step consists in computing

$$\overline{(A_T)}_{ij} = \frac{\exp(-\left\|T \cdot s_i - m_j\right\|^2 / 2\sigma^2)}{\sum_k \exp(-\left\|T \cdot s_i - m_k\right\|^2 / 2\sigma^2)}, \qquad (2)$$

for all pairs (s_i, m_j) and the M-step consists in finding T such that

$$T = \underset{T \in T^*}{\arg\min} \sum_i \left\|T \cdot s_i - \overline{m_i}\right\|^2, \qquad (3)$$

where T^* denotes the set of affine transformations and $\overline{m_i} = \sum_j \overline{(A_T)}_{ij} m_j$ [16]. This amounts to solving a least squares problem.

Once the affine transforms T_P and T_R have been computed for the prostate and the rectum respectively, they can be combined in a unique log-euclidean polyaffine transform as described in [19]:

$$T(x) = \exp\left(w_P(x) L_P x + w_R(x) L_R x\right)$$

Where $\exp(.)$ denotes the exponential map, and w_P, w_R the weights associated with each transform (prostate and rectum resp.).

C. Demons Distance maps Registration

Once the MR prostate and rectum surfaces have been registered on the US image using the EM-ICP scheme of the previous section, a distance map of the new image (i.e representing registered prostate and rectum contours) can be computed. On the other side, the same distance map can be computed for the image which groups together the prostate and rectum surfaces drawn by the surgeon in the course of brachytherapy. In order to improve the polyaffine transformation, a demons registration (see [20]) is then applied taking as fixed image the distance map of the US contours and as moving image, the distance map of the registered MR contours.

III. Experiments and Results

This section reviews the results of the segmentation and registration steps. At each time, the Dice Similarity Coefficient (DSC) was used in order to assess the quality of the step. For two segmentations S1 and S2, the DSC is computed by equation 4. For typical DSC values see for example [21].

$$\text{DSC}(S_1, S_2) = \frac{\text{Volume}(S_1 \cap S_2)}{\frac{1}{2}(\text{Volume}(S_1) + \text{Volume}(S_2))} \qquad (4)$$

Section III-A assess the segmentation step using Dice Similarity Coefficients between our segmentations and expert's MR segmentations. In section III-B, our registration results are assessed. All registration transforms have been computed using our semi-automatic contours obtained on the MR image (see II-A) and the expert's manual contours on the US image. In order to include both segmentation and registration errors, the DSC for the registration part was computed between expert's manual MR contours, after deformation by a transformation computed thanks to the semi-automatic contours, and expert's manual US contours.

A. Segmentation

Segmentation has been applied on a validation set consisting in 5 T2-weighted MR images of size $320 \times 320 \times X$ where X was dependent on each image. Due to the low number of subjects available, we used the first subject as a training to fit the different parameters (σ,λ,...), and we validated the method on the five other subjects. This ensures that the parameters do not overfit the data.

The low resolution segmentation was applied on a subsampled $160 \times 160 \times X$ image and the segmentation was upsampled in order to get the corresponding organ boundaries in the HR image. For the low resolution segmentation, we used pairwise cost std $\sigma = 10$, regional cost weight $\lambda = 0.001$.

The second segmentation was then applied on the multiresolution image using a pairwise cost std $\sigma = 25$ for edges between low resolution voxels solely, and a pairwise cost std $\sigma = 100$ for edges between low and high resolution voxels or between two high resolution voxels. For this second segmentation, we used no regional cost except for the seeds fixed costs (i.e λ was set to zero except for manually selected seeds where it was set to 1).

Results obtained for this multiresolution segmentation were good with mean prostate DSC of 0.72 and mean rectum DSC of 0.78 (table I). One can see that the number of seeds used never exceeds 8% of the prostate (resp. rectum) volume. Mean number of seeds used was of about 5% of total prostate and rectum volumes.

Figure 4 allows a visual assessment of the results. For each patient (P1 to P5), 3 slices were selected as follows. The first and last images correspond to the first and last slices of the prostate manual contour and the second slice is given by round$((z_{first} + z_{last})/2)$ where z_{first} and z_{last} denote the

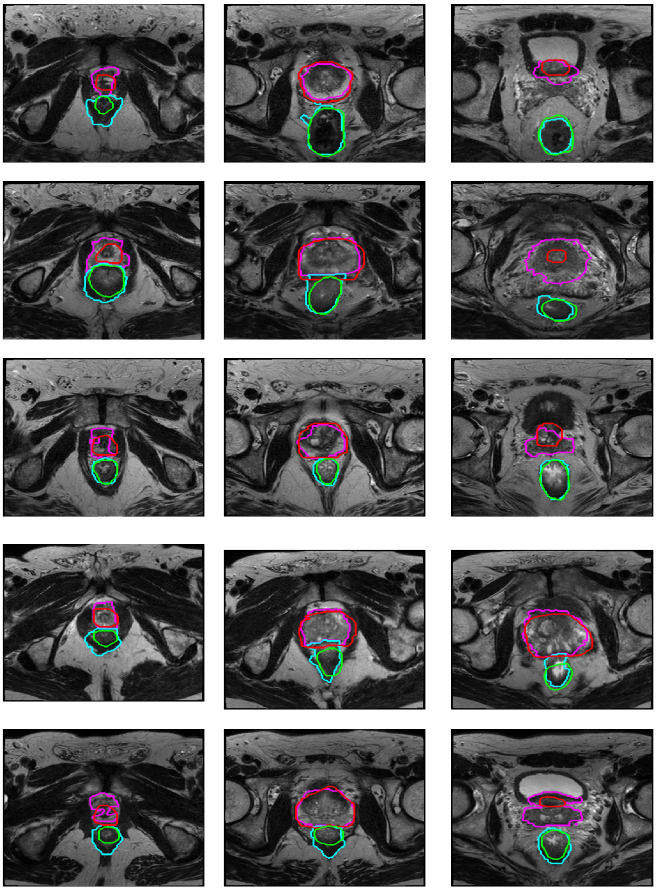

Fig. 4. Results of Multi-resolution image segmentation algorithm for prostate and rectum. *Images show superposition of the prostate and rectum semi-automatic contours (magenta and cyan) as well as expert's manual contours fo both prostate and rectum (red and green resp.) for 3 representative slices of patients P1 to P5 (top to bottom).*

numbers of the first and last slices respectively and round(.) is the nearest integer. As can be seen on those images, results are usually poorer at the base (low discrimination between prostate and urethral bulb) and at the apex (low discrimination between prostate and seminal vesicles) of the prostate. However, keep in mind that the first and last slices are not representative of the whole volume and most of the slices will therefore show a coincidence level close to the coicidence on the middle slice.

TABLE I
SEGMENTATION DSC

	P1	P2	P3	P4	P5	Mean	Std
Prostate	0.75	0.72	0.70	0.72	0.73	**0.72**	**0.02**
Rectum	0.81	0.81	0.90	0.68	0.70	**0.78**	**0.09**
Seeds % pro.	3.1	4.8	4.9	7.8	4.6	**5.04**	**1.7**
Seeds % rect.	1.7	3.7	5.6	7.5	5.1	**4.7**	**2.2**
Seeds % bckg.	0.1	0.2	0.3	0.2	0.2	**0.2**	**0.1**

B. Registration

Affine prostate and rectum registrations were first performed separately. Prostate affine registration was initialized thanks to a first simple rigid registration based on a gradient descent on the US distance map. For the rectum , we extrapolated the partial surface on the US slice assuming it to be part of a circle (namely the probe) and then simply mapped the upper, middle, and lower MR and US contours on each other.

For the registration of rectum surfaces, we used a real noise variance $\sigma^2_{final} = 0.3^2$, initial variance coefficient $a_{init} = 1$, annealing coefficient $c = 1.005$ and maximum Mahalanobis distance $\mu^2_{max} = 0.5$. Namely, when computing the matrix $\overline{(A_T)_{ij}}$ we only considered the points s_i and m_j such that $\|T \cdot s_i - m_j\|^2 < \sigma^2 \mu^2_{max}$. For prostate surfaces, the same algorithm was applied using real noise variance $\sigma^2_{final} = 0.1^2$ initial variance coefficient $a_{init} = 256$, annealing coefficient $c = 1.1$ and maximum Mahalanobis distance $\mu^2_{max} = 0.25$. Again, mean Dice coefficients obtained were good (table II) with mean values of 0.71 (prostate) and 0.68 (rectum). One clearly sees that the deformation underwent by the rectum is non-affine except when the shapes in both images are quite similar (P3 and P5). In the case of the prostate, it seems that the deformation could be defined by a simple affine transformation.

TABLE II
AFFINE REGISTRATION DSC

	P1	P2	P3	P4	P5	Mean	Std
Prostate	0.76	0.71	0.70	0.70	0.69	**0.71**	**0.03**
Rectum	0.66	0.59	0.77	0.66	0.71	**0.68**	**0.07**

After this EM-ICP registration of prostate and rectum, the two affine components were combined in a Log-euclidian polyaffine framework using weights defined by a gaussian of the distance to the prostate and rectum volumes respectively. That is :

$$w_P(x) = \exp\left(-\frac{\min_{p \in V_P} \|x-p\|^2}{2\sigma^2}\right)$$
$$w_R(x) = \exp\left(-\frac{\min_{r \in V_R} \|x-r\|^2}{2\sigma^2}\right). \quad (5)$$

Where V_P and V_R denote the prostate and rectum volumes respectively. The gaussian variance was set to $\sigma^2 = 1.0$.

Finally, registration of distance maps was completed using 4 scales. At each scale, 20 iterations were performed using a gaussian regularization variance $\sigma^2 = 1.5$. Even if we expected some improvement in the DSCs, results were poorer (table III) with mean prostate and rectum DSCs of 0.61 and 0.53 for prostate and rectum respectively.

TABLE III
DEMONS REGISTRATION DSC

	P1	P2	P3	P4	P5	Mean	Std
Prostate	0.56	0.58	0.59	0.67	0.67	**0.61**	**0.05**
Rectum	0.46	0.44	0.70	0.53	0.54	**0.53**	**0.1**

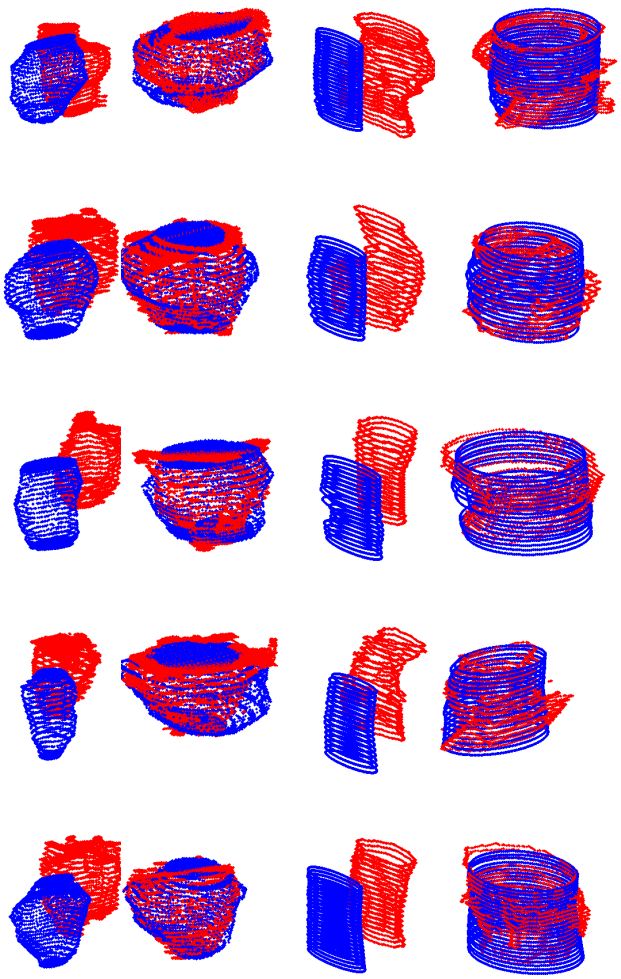

Fig. 5. Results of Affine Registration for prostate and rectum. *Images show prostate surfaces of patients P1 to P5 before and after affine registration (first and second columns) together with rectum surfaces of the same patients before and after affine registration (third and fourth columns).*

IV. Conclusion

In this paper, we proposed a novel approach for MR-US registration in prostate brachytherapy. When applying the affine part of the registration scheme to the prostate, very good DSC were obtained. For the rectum, the deformation between MR and US images was clearly not affine and poorer DSC were obtained. When combining the two affine components in a single log-euclidian polyaffine transform, results became poorer for both prostate and rectum even after application of a demons deformable registration. It therefore seems that prostate and rectum deformations are relatively independent from each other or at least that their interactions cannot be characterized by a polyaffine scheme with gaussian weights.

References

[1] L. Dickinson, H. Ahmed, C. Allen, J. Barentsz, B. Carey, J. Futterer, S. Heijmink, P. Hoskin, A. Kirkham, A. Padhani *et al.*, "Magnetic resonance imaging for the detection, localisation, and characterisation of prostate cancer: Recommendations from a european consensus meeting," *EUROPEAN UROLOGY*, vol. 59, pp. 477–494, 2011.

[2] J. Ferlay, H. Shin, F. Bray, D. Forman, C. Mathers, and D. Parkin, "Estimates of worldwide burden of cancer in 2008: Globocan 2008," *International Journal of Cancer*, vol. 127, no. 12, pp. 2893–2917, 2010.

[3] Z. Wei, G. Wan, L. Gardi, G. Mills, D. Downey, and A. Fenster, "Robot-assisted 3d-trus guided prostate brachytherapy: system integration and validation," *Medical physics*, vol. 31, p. 539, 2004.

[4] M. Vlaardingerbroek and J. Den Boer, *Magnetic resonance imaging: theory and practice*. Springer Verlag, 2003.

[5] E. Haacke, R. Brown, M. Thompson, and R. Venkatesan, *Magnetic resonance imaging: physical principles and sequence design*. Wiley-Liss New York:, 1999, vol. 82.

[6] T. Szabo, *Diagnostic ultrasound imaging: inside out*. Academic Press, 2004.

[7] J. Mitra, A. Oliver, R. Marti, X. Llado, J. C. Vilanova, and F. Meriaudeau, "A Thin-Plate Spline Based Multimodal Prostate Registration with Optimal Correspondences," *Signal-Image Technologies and Internet-Based System, International IEEE Conference on*, vol. 0, pp. 7–11, 2010.

[8] N. Makni, I. Toumi, P. Puech, M. Issa, O. Colot, S. Mordon, and N. Betrouni, "A non rigid registration and deformation algorithm for ultrasound & mr images to guide prostate cancer therapies," in *Engineering in Medicine and Biology Society (EMBC), 2010 Annual International Conference of the IEEE*. IEEE, 2010, pp. 3711–3714.

[9] S. Martin, M. Baumann, V. Daanen, and J. Troccaz, "Mr prior based automatic segmentation of the prostate in trus images for mr/trus data fusion," in *Biomedical Imaging: From Nano to Macro, 2010 IEEE International Symposium on*. IEEE, 2010, pp. 640–643.

[10] B. Porter, D. Rubens, J. Strang, J. Smith, S. Totterman, and K. Parker, "Three-dimensional registration and fusion of ultrasound and mri using major vessels as fiducial markers," *Medical Imaging, IEEE Transactions on*, vol. 20, no. 4, pp. 354–359, 2001.

[11] C. Reynier, J. Troccaz, P. Fourneret, A. Dusserre, C. Gay-Jeune, J. Descotes, M. Bolla, and J. Giraud, "Mri/trus data fusion for prostate brachytherapy. preliminary results," *Medical physics*, vol. 31, p. 1568, 2004.

[12] Y. Boykov and M. Jolly, "Interactive graph cuts for optimal boundary & region segmentation of objects in ND images," in *Computer Vision, 2001. ICCV 2001. Proceedings. Eighth IEEE International Conference on*, vol. 1. IEEE, 2001, pp. 105–112.

[13] Y. Boykov, O. Veksler, and R. Zabih, "Efficient approximate energy minimization via graph cuts," *IEEE Transactions on Pattern Analysis and Machine Intelligence*, vol. 20, no. 12, pp. 1222–1239, 2001.

[14] V. Kolmogorov and R. Zabin, "What energy functions can be minimized via graph cuts?" *Pattern Analysis and Machine Intelligence, IEEE Transactions on*, vol. 26, no. 2, pp. 147–159, 2004.

[15] Y. Boykov and V. Kolmogorov, "An experimental comparison of min-cut/max-flow algorithms for energy minimization in vision," *Pattern Analysis and Machine Intelligence, IEEE Transactions on*, vol. 26, no. 9, pp. 1124–1137, 2004.

[16] S. Granger and X. Pennec, "Multi-scale EM-ICP: A fast and robust approach for surface registration," *Computer VisionECCV 2002*, pp. 69–73, 2006.

[17] O. Commowick, V. Arsigny, A. Isambert, J. Costa, F. Dhermain, F. Bidault, P. Bondiau, N. Ayache, and G. Malandain, "An efficient locally affine framework for the smooth registration of anatomical structures," *Medical Image Analysis*, vol. 12, no. 4, pp. 427–441, 2008.

[18] Y. Boykov and O. Veksler, "Graph cuts in vision and graphics: Theories and applications," *Handbook of Mathematical Models in Computer Vision, Springer-Verlag*, pp. 79–96, 2006.

[19] V. Arsigny, O. Commowick, N. Ayache, and X. Pennec, "A fast and log-euclidean polyaffine framework for locally linear registration," *Journal of Mathematical Imaging and Vision*, vol. 33, no. 2, pp. 222–238, 2009.

[20] X. Pennec, P. Cachier, and N. Ayache, "Understanding the demons algorithm: 3D non-rigid registration by gradient descent," in *Medical Image Computing and Computer-Assisted Intervention–MICCAI99*. Springer, 1999, pp. 597–605.

[21] M. Foskey, B. Davis, L. Goyal, S. Chang, E. Chaney, N. Strehl, S. Tomei, J. Rosenman, and S. Joshi, "Large deformation three-dimensional image registration in image-guided radiation therapy," *Physics in Medicine and Biology*, vol. 50, p. 5869, 2005.